Egypt. J. Chem. **Vol. 62**, No. 2 pp. 311 - 323 (2019)

Optical Characterization of Poly [2-methoxy-5-(2-ethylhexyloxy-p-phenylene Vinylene] (MEH-PPV):C_{60}, MEH-PPV:C_{60}:TiO_2 and MEHPPV:C_{60}:ZnO Thin Films

Fawzy A. Mahmoud[1], Islam A. Elazab*[2], Ossama M. Abo-Elenien[3], Ahmed Abdel Fatah[2], Adel A. M. Ahmed[2]

[1]Physics, Solid Physics Department, National Research Centre (NRC), Cairo, Egypt.
[2]Chemistry Department, Faculty of Science, Helwan University Cairo, Egypt.
[3]Petroleum Applications Department, Egyptian Petroleum Research Institute (EPRI) Cairo, Egypt.

IN THIS WORK, ZnO and TiO_2 nanoparticles were prepared separately by sol gel method. Structural, morphological and optical properties of both of them are studied. A hexagonal crystal structure of ZnO was formed, while different weight ratio of Anatase (85%) and rutile (15%) phases of TiO_2 nanoparticles were formed as confirmed by the X-ray diffraction (XRD). In addition, The XRD and Raman spectroscopy showed that our materials are polycrystalline. The particles sizes were calculated by sheerer formula are found to be closed to that got from scanning electron microscope (SEM) and transmission electron microscope (TEM). The band gaps for both materials were calculated from Kubelka-Munk function using their measured diffuse reflection. The band gap for ZnO and TiO_2 nanoparticles found to be 3.4 eV and 3.2 eV respectively. Poly [2-methoxy-5-(2-ethylhexyloxy-p-phenylene-vinylene] which named MEH-PPV with C_{60} were dissolved and spin coated on glass substrates to get thin film. Structural, morphological and optical properties of this thin film were studied. Also, the effects of adding any of our metal oxides nanoparticles (ZnO or TiO_2) on the physical properties of MEH-PPV:C_{60} are studied. All results are correlated to check the applicability of using these layers as an absorber layer for solar energy applications.

Keywords: Ternary composite, MEHPPV, C_{60}, TiO_2 nanoparticles, ZnO nanoparticles, Thin film .

Introduction

Titanium dioxide (TiO_2) and Zinc oxide (ZnO) nanoparticles (NPs) are oxides semiconductor of important interest in many fields of applications. In particular, solar cells [1,2]. They are naturally occurred, inexpensive, nontoxic and possess good physical and chemical properties [3-5]. Zinc oxide nanoparticles (ZNPs) and Titanium dioxide nanoparticles (TNPs) have wide electronic band gaps of 3.37 eV [6] and 3.2 eV [7], respectively. The most common ZnO structure is the hexagonal wurtzite structure due to its stability at ambient conditions [8]. Rutile, anatase and brookite are the three phases of TiO_2 in the order of abundance [9]. Anatase phase TiO_2 is preferred for optoelectronic applications rather than rutile phase TiO_2, owing to its better electron transport and reduced charge carrier recombination [10]. ZNPs and TNPs can be prepared in different structural shapes such as sphere, sheet, flower, rod, wire, etc. [11, 12]. The optical and electrical properties of ZnO and TiO_2 nanostructures strongly depend on their crystalline structure, morphology, defects and impurity contents which in turn depends on the preparation method [12,13]. In many literatures, various techniques are being used to synthesize ZNPs and TNPs. Among that, the sol-gel method considered as an attractive method because of its simplicity, low power consumption, low temperature required, and controllable final product properties [7, 14].

Conjugated polymers are polymers containing highly loosely held electrons in their backbones, or organic macromolecules that consist one backbone chain of alternating double and single bonds, sometimes referred to as conducting

*Corresponding author e-mail: islam.a.azab@gmail.com; Tel.: +201002083664
DOI: 10.21608/EJCHEM.2018.4816.1426

polymers. Conjugated polymers are of two types, π-conjugated and homo-conjugated polymers. The π-conjugated polymers attracted much research efforts after the discovery that their electrical conductivity increases substantially upon electrochemical doping. The goal of using such materials is to obtain optoelectronic or photovoltaic cells at low costs and/or obtain new device functionalities (e.g., impact resistance, mechanical flexibility, and optical transparency) that are challenging to achieve with other types of materials e.g. Silicon. Poly phenylene vinylene (PPV) and its derivatives exhibit luminescence at red emission of the visible spectrum and have been widely studied as potential candidates for the fabrication of optoelectronic devices. A range of photophysical and electronic properties have been achieved by varying the functional groups along the PPV backbone. In particular, MEH-PPV is a π-conjugated conducting polymer and mainly used in the fabrication of Light emitting diodes (LEDs) and photovoltaic cells [15]. The polymer thin films affected by the polymer morphology and its processing conditions [15]. Composites of MEH-PPV: Fullerene molecules (C_{60}) possess a good electrical, optical and mechanical properties [16].

In this work, the sol–gel method was used to prepare ZNPs and TNPs. The prepared nanoparticles characterized using Fourier Transform Infrared Spectroscopy (FTIR), X-ray Diffraction (XRD), Raman-Scattering, Scanning Electron Microscopy (SEM), Transmission Electron Micrograph (TEM), Energy Dispersive X-ray Analyzer (EDX), UV-VIS-NIR spectrophotometer and Photoluminescence measurements. Composites thin films of MEH-PPV:C_{60}, MEH-PPV:C_{60}:TiO_2 and MEH-PPV:C_{60}:ZnO were prepared by spin coating on glass substrate. Structural, morphological and optical properties of the three thin films were studied to measure the effect of adding inorganic NPs.

Experimental

Materials

The MEHPPV, C_{60}, Zinc acetate, Sodium hydroxide (NaOH), Titanium tetra iso propoxide [$Ti(OCH(CH_3)_2)]_4$, 97%], nitric acid [HNO_3] and all solvents including acetone, ethanol, iso-propanol [$(CH3)_2CHOH$] were purchased from Sigma Aldrich company and used without further purification. All chemicals were reagent grade. Distilled water was used throughout the experiments.

Preparation of ZnO nanoparticles

The sol-gel method was used to synthesize zinc oxide nanostructure [17]. 8 g of NaOH was dissolved in a 10 ml of distilled water and 2 g of zinc acetate dihydrate was dissolved with a 15 ml of distilled water. Both solutions separately were stirred for about five minutes. After well mixed, NaOH solution was poured to the zinc acetate solution with magnetic stirring for five minutes. Then, 100 ml of ethanol was added dropwise to the solution containing both zinc acetate and NaOH solution. White precipitate was formed after the reaction was completed.

Preparation of TiO_2 nanoparticles

Titanium Oxide nanostructure was synthesized by using sol-gel method [18]. A 20 ml of Titanium tetra iso propoxide [TTIP] solution was added drop wise into the 22 ml of solution containing 10 ml of iso-propanol and 12 ml deionised water with stirring at 80º C for 1 h. After that, 8 ml concentrated HNO_3 mixed with deionized water was added into the TTIP solution with constant stirring at 60 ºC for 6 h. Sol gel was obtained. Which then heated at 300 ºC for 2 h. After annealing, the TiO_2 nanocrystalline was obtained.

Preparation of thin films

Glass substrates were cleaned by using acetone then ethanol for 10 minutes each with sonication. MEHPPV (0.015gm) and C_{60} (0.009gm) were dissolved in chloroform (1ml). The mixture solution then sonicated for 15 min after that stirred for 30 min on hot plate at 50. The prepared solution was applied by spin coater onto the cleaned glass substrate surface at 2000 rpm for 60 seconds to form the blank sample. Finally, the substrate was heated at 50 for 15 minutes [19].

The ternary composite samples were prepared by firstly adding ZnO nanoparticles (0.0045gm) or TiO_2 nanoparticles (0.0045gm) to Chloroform (1ml) and sonicated for 30 minutes to improve the dispersion of the nanoparticles. MEHPPV (0.015gm) and C_{60} (0.0045gm) then added to the solution and sonication occurred. After that the whole mixture stirred on hot plate and heated at 50. Then, the two ternary composites were applied by spin coater onto the cleaned glass substrate surface at 2000 rpm for 60 seconds. The formed thin films (TFs) were heated at 50 for 15 minutes [20].

Characterization of TiO_2 and ZnO nanoparticles

The size and morphology of ZNPs and TNPS were obtained by Transmission Electron Microscope (TEM) using JEM-2100 (JEOL-Electron Microscope) and Scanning Electron Microscope (SEM) using SEM-JEOL (JXA-840A Electron Probe Microscope). The samples for SEM were coated with gold and the samples for TEM analysis were prepared by dropping dilute suspension of ZNPs and TNPs onto copper grids. The chemical composition of the prepared nanoparticles was carried out by JEOL [JXA-840A energy dispersive X-ray analyzer (EDX)] attached to SEM. To confirm the structure properties of the prepared nanoparticles, the X-ray diffraction (XRD) was performed at room temperature using A Philips (X ˜ Pert Multi-Purpose diffraction) operated at 40 kV/30 mA. The crystals size was calculated by Scherrer's formula. Fourier Transform Infra-Red (FTIR) spectra were measured on Jasco 6100 Japan spectrometer with a wave number range of 400 to 4000 cm^{-1} to identify the presence of chemical groups present in the synthesized nanoparticles. In addition, the Raman-scattering measurements were carried out using Dispersive Raman Microscope (Bruker-Senterra), (λ = 532 nm) at room temperature. The prepared nanoparticles samples were dispersed in ethanol and stirred vigorously for homogeneous dispersion to obtain Photoluminescence (PL) spectrum by using Jasco FP-6500 Japan spectrofluorometer at room temperature. Finally, at room temperature JASCO-(670) UV-VIS-NIR spectrophotometer was used to obtain the diffuse reflectance in the wavelength range 200-2500 nm.

Characterization of thin films

The surface morphology of the prepared TFs, MEH-PPV:C_{60}, MEH-PPV:C_{60}:TiO_2 and MEH-PPV:C_{60}:ZnO were characterized using SEM-JEOL (JXA-840A Electron Probe Microscope) operated at a voltage of 20 kV. The SEM samples were coated with gold using low voltage sputtering. The optical transmission and reflection were measured using JASCO-(670) UV-VIS-NIR spectrophotometer in the wavelength range 200-2500 nm. The PL for the composite films obtained using Jasco FP-6500 Japan spectrofluorometer at room temperature. The XRD was performed at room temperature using A Philips (X ˜ Pert Multi-Purpose diffraction) operated at 40 kV/30 mA to confirm the structure properties of the prepared composites. Finally, FTIR spectra were measured on Jasco 6100 Japan spectrometer with a wave number range of 400 to 4000 cm^{-1}.

Results and Discussion

Figure 1 shows XRD patterns of TNPs, MEH-PPV:C_{60} TF & MEH-PPV:C_{60}:TiO_2 TF (a) and ZNPs, MEH-PPV:C_{60} TF & MEH-PPV:C_{60}:ZnO TF (b) in the wide-angle range of 2θ ($20° < 2\theta < 90°$). The peaks miller indices [hkl] assignment indicated on both figures. The diffraction lines of TNPs, (Fig.1a), confirm the presence of the anatase phase (JCPDS 01-075-2552). Furthermore, show three peaks assigned to the rutile phase (JCPDS 01-071-4809). This indicates that TNPs sample contains small amount of rutile TiO_2. The weight ratio of the anatase and rutile phases are 85% and 15%, respectively. The weight ratio was calculated by using of the following equation:

$$WR = \frac{Ar}{0.884Aa + Ar} \qquad (1)$$

where A_r represents the integrated intensity of the rutile (110) peak, and A_a is the integrated intensity of the anatase (101) peak. The sharpness, strong intensity and narrow width of ZNPs diffraction peaks, (Fig. 1b), indicate that the synthesized ZNPs sample is well crystallized and in a pure form (JCPDS 01-074-9939). The (101) plane for anatase phase and (110) plane for rutile phase were chosen to calculate the crystalline size, which were found to be 24.42 and 29.35 nm, respectively. While that for ZNPs were 40.7 nm. The crystalline size (D) determined by the Scherrer's formula:

$$D = \kappa \lambda / (\beta \cos\theta) \qquad (2)$$

Where λ is the wavelength of X-ray radiation (Cu$\kappa\alpha$ = 0.15406 nm), is a constant taken as 0.89, β is the line width at half maximum height (FWHM) of the peak, and θ is the diffracting angle. The XRD patterns in Fig. a and b for MEH-PPV:C_{60}:TiO_2 and MEH-PPV:C_{60}:ZNPs TFs show no distinct peak, which ascertain a complete dispersion of the NPs with the polymer matrix. Figure 2 illustrates the infrared spectrogram of TNPs (a), ZNPs (b) and TFs (c) in the range of 400–4000 cm^{-1}. The broad bands appeared for TNPs and ZNPs around 3383 and 3408 cm^{-1}, respectively, are attributed to the O-H stretching mode of the surface adsorbed moisture water molecules, which is supported by other bands at 1631 and 1590 cm^{-1} for the O-H bending mode [21, 22]. The band at 2922.36 cm^{-1} (TNPs) and those at 2924 and 2854 cm^{-1} (ZNPs) are attributed to the C-H stretching band, which means there is a trace from organic compounds.

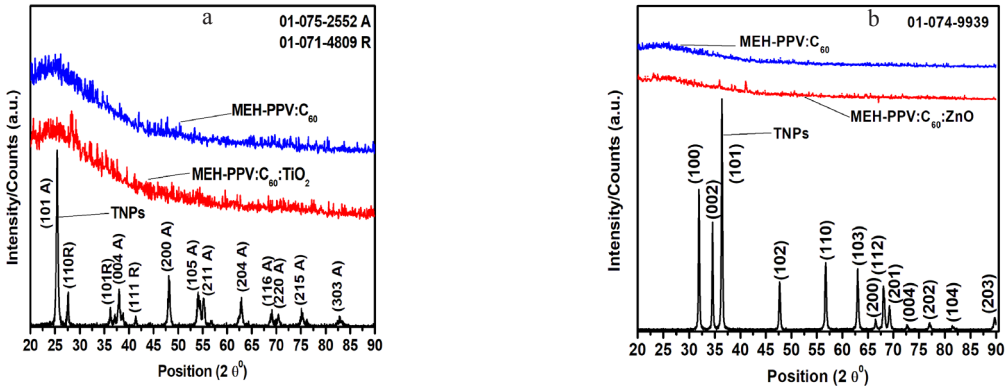

Fig. 1. XRD patterns of TNPs, MEH-PPV:C_{60} TF & MEH-PPV:C_{60}:TiO_2 TF (a) and ZNPs, MEH-PPV:C_{60} TF & MEH-PPV:C_{60}:ZnO TF (b)

The band observed at 703.02 cm^{-1} is due to the Ti-O-Ti bond stretching mode [21]. On the other hand, a significant band found at 543 cm^{-1}, which is the characteristic stretching vibration of Zn-O bond [22]. The FTIR spectra of TFs appeared in Fig. 2 c. The MEH-PPV characteristics peaks are the same in the three composites TFs [23]. The stretching O-H band appeared at 3424 cm^{-1}, with another characteristic stretching peak at 1675.8 cm^{-1}. The peak at 3058.55 cm^{-1} is for the asymmetric stretching vibration of C-H, the peaks at 2956.34, 2927.41 and 2865.7 cm^{-1} are assigned for the symmetric stretching band of -CH_2. The three peaks located at 1413.57, 1504.2, and 1592.91 cm^{-1} are for the stretch modes associated with the phenyl ring. The two modes of the C-O single bonds appeared, the one at 1205.29 is related to the phenyl-oxygen stretch, and the other one at 1041.37 is due to the O-alkyl modes i.e., the oxygen-methyl bond and the oxygen-ethylhexyl. The peak appeared at 968.09 cm^{-1} due to the olefinic trans—CH wag which characterizes the polymer conjugation while the bands appeared at 860.096 cm^{-1} 1384.64 and 1461.78 cm^{-1} are related to out of plane CH wag, symmetric and the asymmetric signatures for CH_2, CH_3. The C_{60}

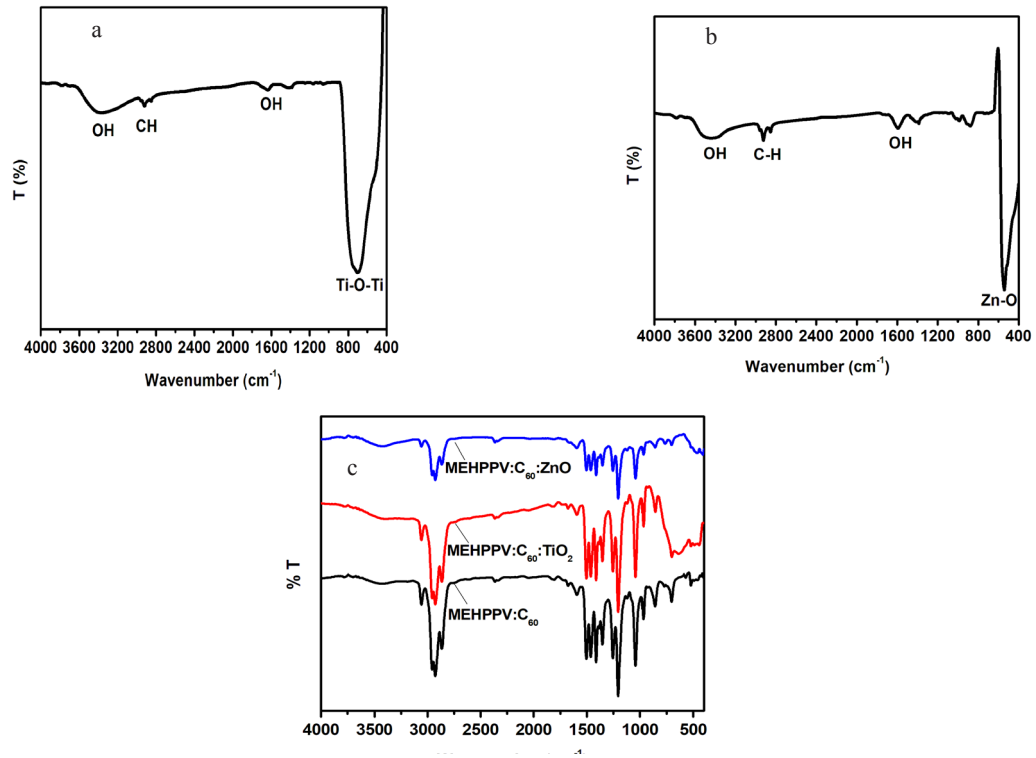

Fig. 2. FTIR spectrogram of TNPs (a), ZNPs (b) and TFs (c).

characterized by three peaks appeared at 524, 1219, and 1456 cm^{-1} [24]. The peak appeared at 701.96 cm^{-1} assigned for Ti-O-Ti (Red line) and that at 460 cm-1 assigned for the Zn-O (blue line) [21, 22].

Raman spectra confirm the anatase structure of the TNPs as shown in Fig. 3 a. The rutile phase was not detected, probably because of its small concentration and its lower Raman scattering efficiency compared to the intense anatase one. The Raman active modes for anatase are evident as an intense peak around 142.12 cm^{-1} (E_g) as well as three other peaks at 395.28 (B_{1g}), 515.92 (A_{1g}) and 636.97 cm^{-1} (E_g) present, this in agreement with other Raman analysis for the anatase phase of TNPs [25]. The Raman-scattering spectra of ZNPs are shown in Fig. 3 b. The main sharp peak located as 437 cm^{-1} [E2H] is the Raman active characteristic optical phonon mode of the wurtzite hexagonal phase ZnO. Other peaks also observed at 100.8 cm^{-1} [E2 Low], the peak at 331.9 cm^{-1} arises from the zone boundary phonons [3E2H–E2L], the peak at 388 cm^{-1} [A1T], [26]. The peaks at 209.4, 538.7, 580.9, 657.6, 1106 and 1152 are assigned to [2E2L] second order phonon mode, [2LA], [E1(To)], an acoustic overtone with A1 symmetry, A1/E2 symmetry and 2LO modes, respectively, [27, 28]. The high intensity peak observed at 437 cm^{-1} in comparison with the other peaks, proved that the ZNPs are of wurtzite hexagonal phase with good crystallinity. There

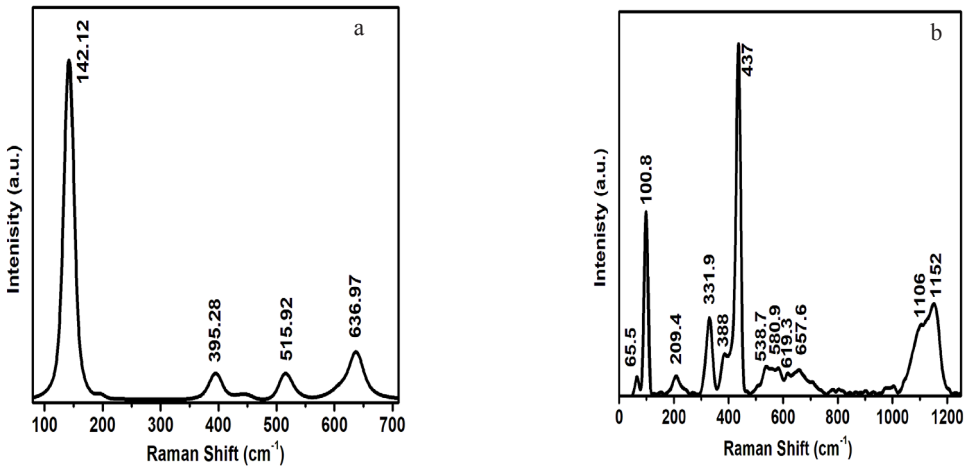

Fig. 3. Raman spectra of TNPs (a) and ZnO (b)

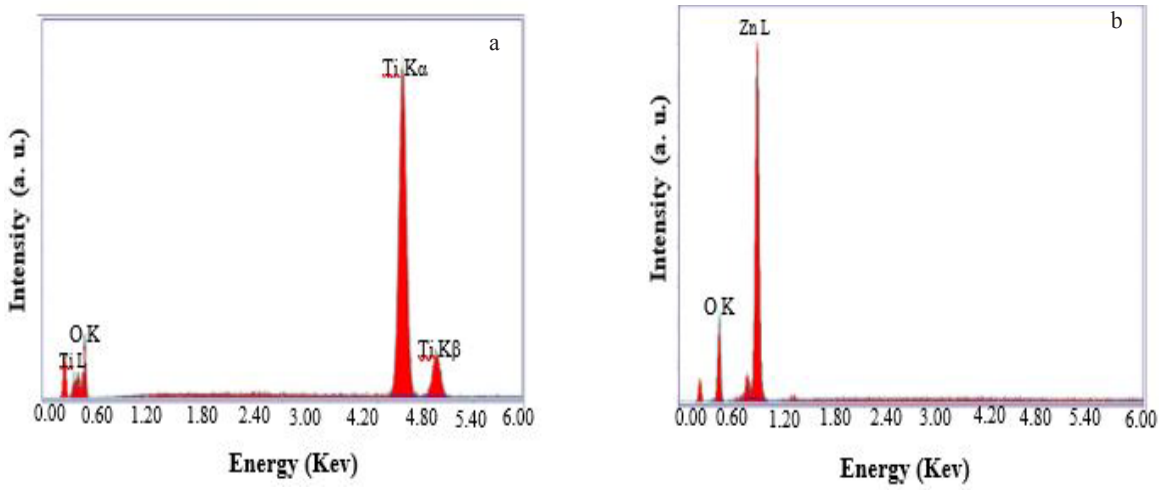

Fig. 4. EDX spectrum for TNPs (a) and ZNPs (b)

also seems to be a weak feature around 800 and 1000 cm^{-1} but it is too small to really be analyzed with any accuracy. There is no impurity peak was observed in the EDX spectra of TNPs and ZNPs, (Fig. 4 a & b). This confirms that the prepared samples are in pure form.

Both SEM and TEM images show that TiO_2 and ZnO are in the nanoscale which is in good agreement with the data obtained from the Scherrer's formula (Fig. 5 a, b, c and d). From Fig. 5 a & c, TNPs are spherical in shape and exhibited irregular morphology due to some agglomeration of primary particles. From Fig. 5 b & d, nearly all the ZNPs are spherical in shape and evenly distributed. Figure 5 e shows that the MEH-PPV:C_{60} are properly mixed and form homogenous TF on the glass substrate. It is clear from Fig. 5 f & g that the addition of TNPs and ZNPs increase the roughness of the polymer film and form aggregates in some regions, TNPs show less aggregation and both NPs evenly distributed through the formed films.

In Fig. 6 a, the visible luminescence band of TNPs located at 405 nm (3.06 eV) is relative to anatase structure. The multi-peak Gauss fitting of the broad emission band gives three Gaussian sub-bands located at 403 nm (3.08 eV), 432 nm (2.87 eV) and 491 nm (2.53 eV). The three sub-band attributed to self-trapped excitons, Ti^{3+} states and the deep-trap state associated with the F^+ center, respectively**.** Ti^{3+} and F^+ centers formed because of the loss of an oxygen atom [29]. Three bands appeared for ZNPs, one located at 412 nm (3.01eV) for ultraviolet emission, the second band located at 436 nm (2.85eV) represents the blue emission and the third shoulder band located at 503 nm (2.47eV) for the green emission, (Fig. 6 b). An electron transition from a shallow donor level of neutral zinc interstitial to top level of the valance band cause the ultraviolet emission. The blue emission ascribed to the recombination between zinc interstitial (Zn_i) energy level to zinc vacancy (V_{Zn}) energy level and the green emission was due to the recombination between the conduction band and the zinc vacancy [30].

Figure 6 c, shows the PL spectra of MEH-PPV:C_{60}, MEH-PPV:C_{60}:TiO_2 and MEH-PPV:C_{60}:ZnO. The characteristic PL peaks are observed around 590 and 633 nm for MEH-PPV:C_{60}. These peaks are attributed to the emission of the PPV backbone as a result of the excited π-electrons relaxation to the ground state and the interchain states [31], respectively. The main peak at 590 nm quenched upon the addition of TNPs and ZNPs to the composite of MEH-PPV:C_{60} with a little variation in the shoulder peak. This is attributed to the charge transfer between MEH-PPV:C_{60} and TNPs or ZNPs. The degree of the PL quenching is an indication of how well the nanoparticles are mixed in the MEH-PPV:C_{60} and the quality of the interface between polymer nanoparticles. A small red shift observed upon incorporation of NPs to the MEH-PPV:C_{60} composite due to the formation of new bonds between a polymer chain and the NPs that altering the electronic configuration of the polymer chain and its conjugation length.

The optical transmittance (T) and reflectance (R) measurement carried out at room temperature for NPs and TFs, (Fig. 7 a-h). As seen from the spectra, the diffuse reflectance for NPs samples possesses high values at the visible region reaches between 85-90% and decrease with increasing wavelength in the range of 600 – 2500 nm, (Fig. 7 a & b). In Fig. 7 c, d & e, the reflectance of the MEH-PPV:C_{60} TF decreased after the addition of TNPs and ZNPs at the visible region. Low reflectance values indicate high absorption in the corresponding wavelength region. The transmittance spectra of MEH-PPV:C_{60}, MEH-PPV:C_{60}:TiO_2 and MEH-PPV:C_{60}:ZnO TFs show that the average value of transmittance was about 40% , 18% and 20% respectively, in the visible range of electromagnetic radiation. While the transmittance values increase at the near infra-red region. The slightly lower values of transmittance in case of the two ternary films could be due to light scattering at the rough surface due to the incorporation of ZNPs and TNPs [32]; this is in good agreement with data obtained from SEM images.

The band gap energy for TNPs and ZNPs can be determined by using the modified Kubelka-Munk function $[F(R)\ h\nu]^n$, (Fig. 8 a & b). Where R is the reflectance, F(R) is proportional to the extinction coefficient (α) and (n) associated with an electronic transition. While Tauc's Model is employed as can be seen in Fig.8 c, d & e, in order to quantify the optical band gap of TFs. where α is the absorption coefficient and $h\nu$ is the photonic energy. Assuming direct allowed transition (n=2), the values of direct band gap were obtained from the linear portion of the plot of $(F(R)\ h\upsilon)^2$ or $(\alpha h\upsilon)^2$ Vs. $h\nu$ when extrapolating to zero. The result showed the optical band gap is found to be 3.2 [33], 3.4 [32], 2.2, 2.1 and 2.08 eV for TNPs, ZNPs, MEH-PPV:C_{60}, MEH-PPV:C_{60}:TiO_2 and

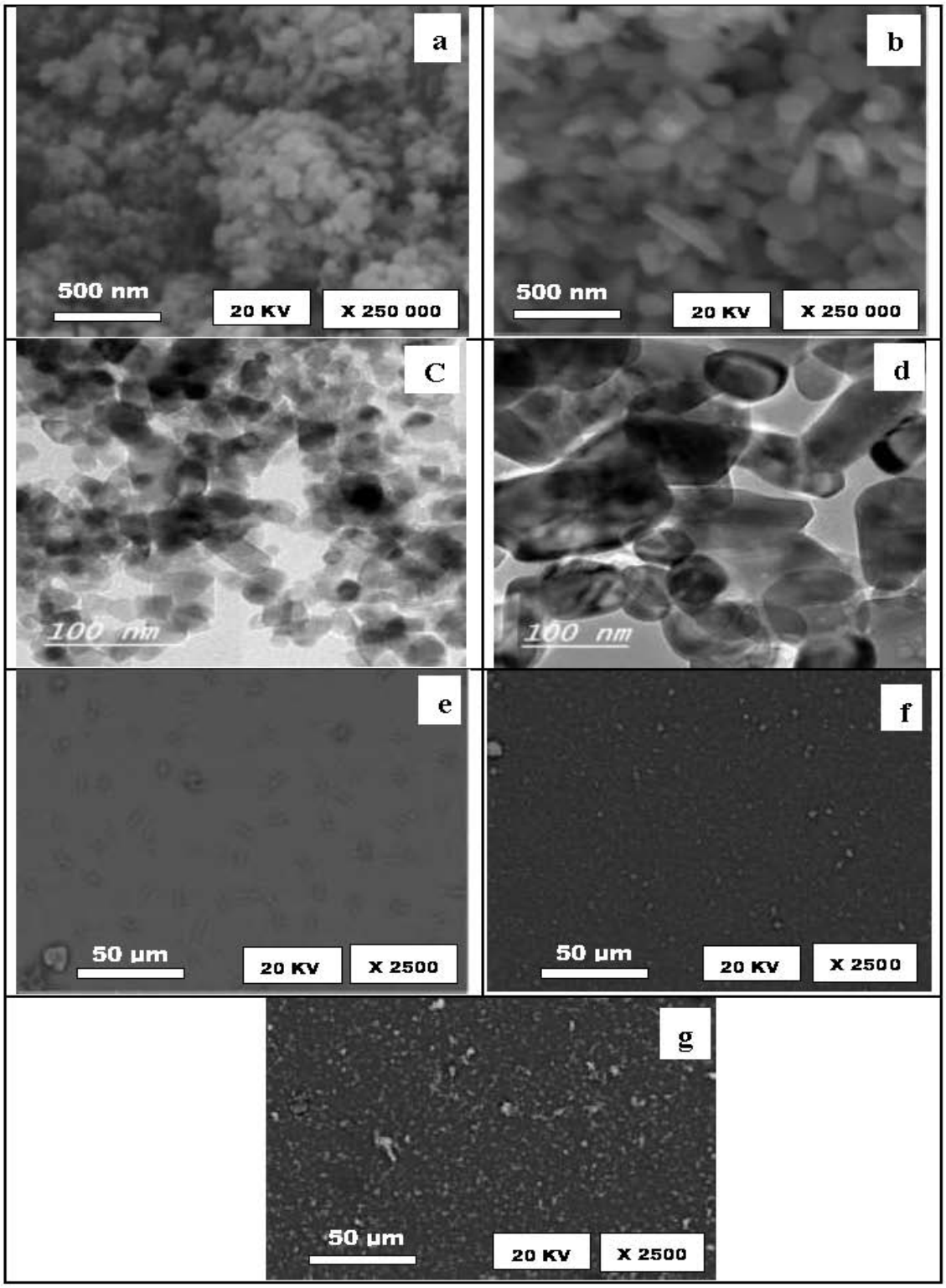

Fig. 5. SEM Microgram of TNPs (a), ZNPs (b), TEM Microgram of TNPs (c), ZNPs (d) and SEM Microgram of MEH-PPV:C_{60} (e), MEH-PPV:C_{60}:TiO_2 (f) and MEH-PPV:C_{60}:ZnO (g)

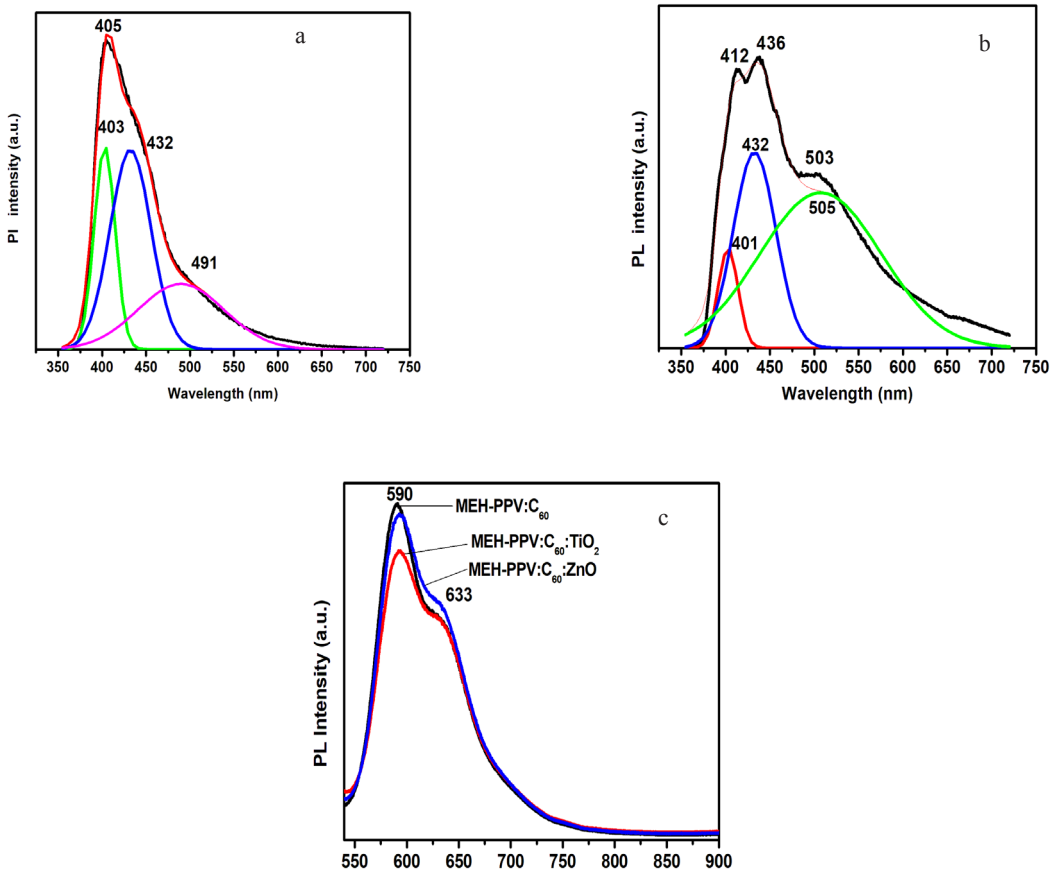

Fig. 6. Photoluminescence spectra of TNPs (a), ZNPs (b) and TFs (c)

MEH-PPV:C_{60}:ZnO respectively. Also, it is clear that the optical band gap of MEH-PPV:C_{60} can be tuned by introducing of TNPs and ZNPs. The small value of optical band gaps means that it is easy for electrons to absorb a photon (light) to jump from the valence band to conduction band. The presence of ZNPs and TNPs cause a shift in the optical band gap, which may be ascribed to the band shrinkage effect due to increasing carrier concentration. The obtained low band gap shows that the synthesized polymer may be suitable for solar cell application.

Conclusion

TiO_2 and ZnO nanoparticles have successfully synthesized using the sol gel method and characterized with different characterization techniques. The XRD gave the main characteristics peaks for TiO_2 and ZnO structure. In addition, the FTIR spectra and Raman spectra confirmed the formation of TiO_2 and ZnO nanoparticles. The SEM and TEM analysis for TNPs and ZNPs showed that TNPs were spherical in shape, but in the case of ZNPs most of them were spherical in shape. Added to the previous, both TNPs and ZNPs were in the nanoscale size, which in good agreement with the data obtained from the Scherrer's formula. The EDX analysis confirmed that the prepared NPs samples were in pure form. MEH-PPV, C_{60} and inorganic semiconductor nanoparticles (TiO_2 or ZnO) dissolved, mixed and spin-coated on cleaned glass substrate. The incorporation of the NPs changed the morphology and increased the roughness of polymers film (MEH-PPV:C_{60}) as showed by the SEM images. Characterization by FTIR and XRD confirmed that the NPs have incorporated within the polymer matrix. The PL quenching provided evidence of photoinduced charge transfer within the ternary composites. The optical band gap of the MEH-PPV:C_{60} slightly decreased after the addition of TNPs and ZNPs

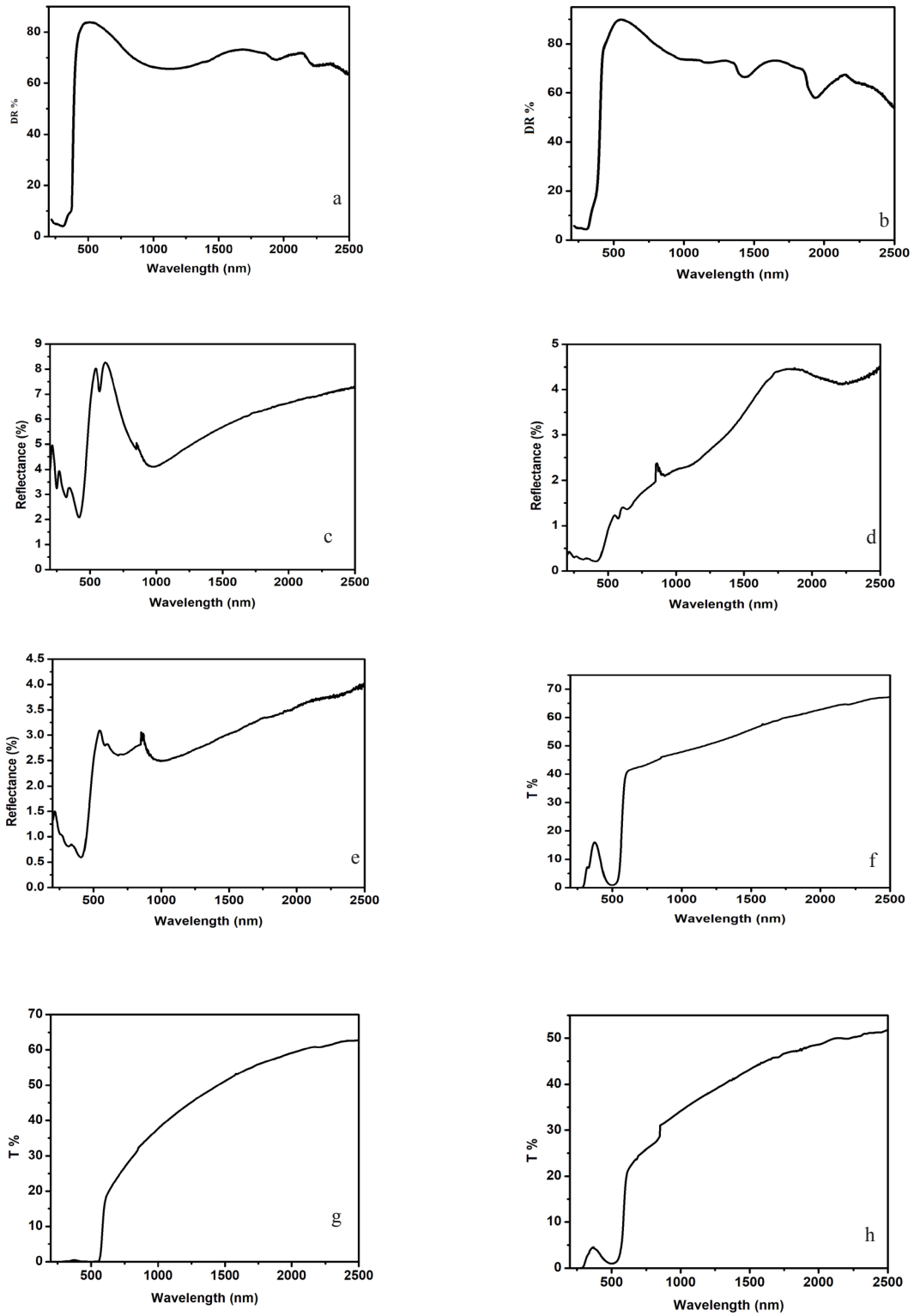

Fig. 7. Diffused reflectance of TNPs (a), ZNPs (b) and the specular reflectance of MEH-PPV:C_{60} (c), MEH-PPV:C_{60}:TiO_2 (d) and MEH-PPV:C_{60}:ZnO (e) and Transmittance of MEH-PPV:C_{60} (f), MEH-PPV:C_{60}:TiO_2 (g) and MEH-PPV:C_{60}:ZnO (h).

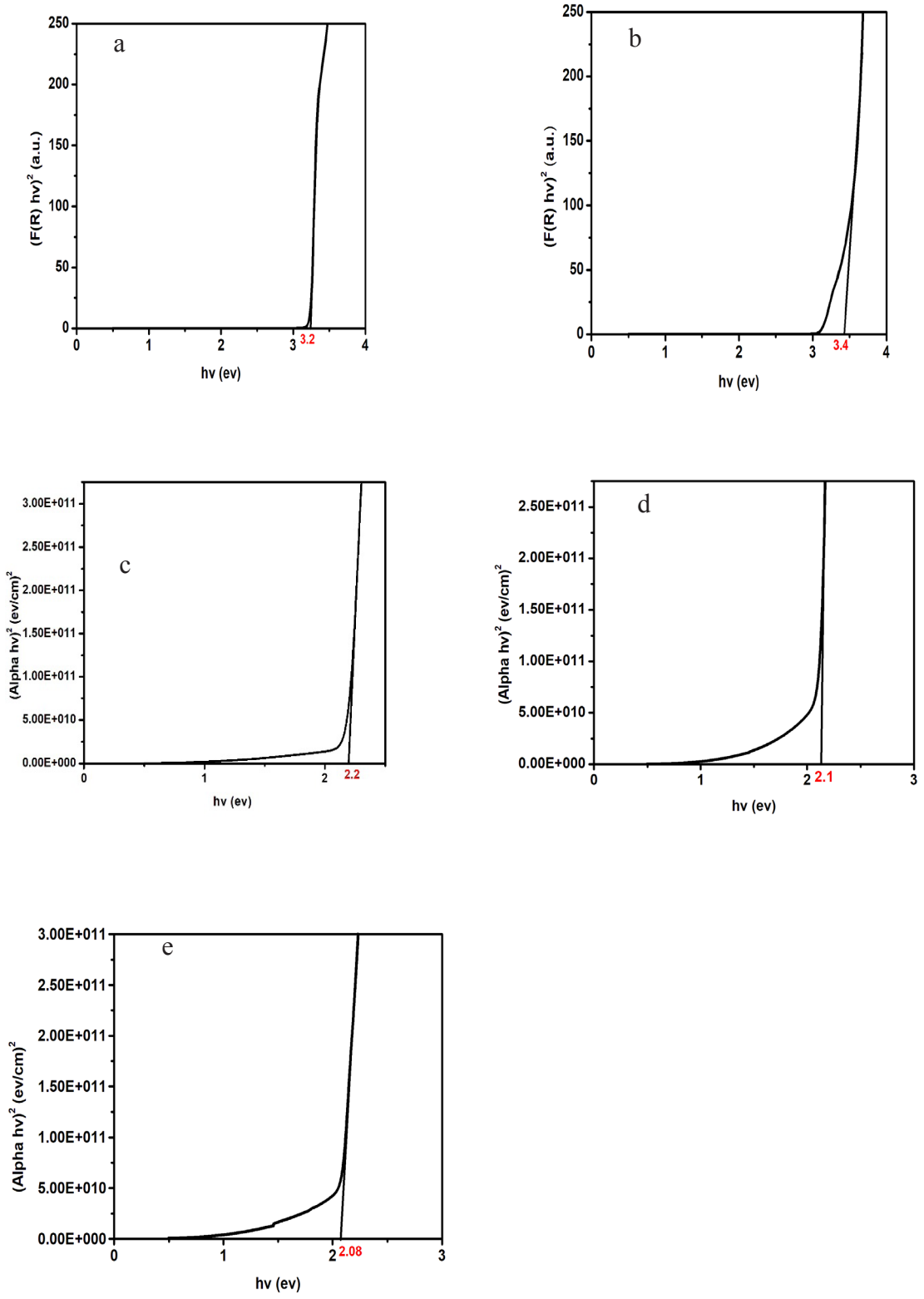

Fig. 8. Talc's plot of TNPs (a), ZNPs (b), MEH-PPV:C_{60} (c), MEH-PPV:C_{60}:TiO_2 (d) and MEH-PPV:C_{60}:ZnO (e)

and found to be 2.1 and 2.08 eV respectively and thus give a better performance to the thin films. The study showed that the presence of TNPs and ZNPs in the polymeric film improved the optical characteristics of MEH-PPV:C_{60} and gives information on the possibility of application in solar energy applications.

References

1. Habelhames F., Wided Z., Lamiri L., Nessark B. and Derbal-Habak H., Morphology and photoelectrochemical characterization of MEH-PPV/PCBM composite film doped with TiO_2 nanoparticles. *Acta Metallurgica Sinica (English Letters)*, **26**(4), 373-377 (2013).
2. Huang J., Yin Z. and Zheng Q., Applications of ZnO in organic and hybrid solar cells. *Energy & Environmental Science*, **4**(10), 3861-3877 (2011).
3. Shon H., Phuntsho S., Okour Y., Cho D. L., KK S., Li J. H., Na S.H., Kim J.B. and Kim J. H., Visible light responsive titanium dioxide (TiO_2). *Journal of the Korean Industrial and Engineering Chemistry,* (2008).
4. Janotti A. and Van de Walle C. G., Fundamentals of zinc oxide as a semiconductor. *Reports on Progress in Physics*, **72**(12), 126501 (2009).
5. Znaidi L., Touam T., Vrel D., Souded N., Ben Yahia S., Brinza O., Fischer A. and Boudrioua A., ZnO thin films synthesized by sol-gel process for photonic applications. *Acta Physica Polonica-Series A General Physics*, **121**(1), 165 (2012).
6. Athare A. E., Synthesis and Characterisation of ZnO Nanoparticals by XRD, EDX, SEM, FTIR and UV-DRS. *IJSRSET*, **4**(1), 627-631(2018).
7. Bagheri S., Shameli K. and Abd Hamid S. B., Synthesis and characterization of anatase titanium dioxide nanoparticles using egg white solution via Sol-Gel method. *Journal of Chemistry*, Volume 2013, Article ID 848205, 6 pages (2012).
8. Ashrafi A. B. M. A. and Jagadish C., Review of zincblende ZnO: stability of metastable ZnO phases. *Journal of Applied Physics*, **102**(7), 4 (2007).
9. Shirke B. S., Korake P. V., Hankare P. P., Bamane S. R. and Garadkar K. M., Synthesis and characterization of pure anatase TiO_2 nanoparticles. *Journal of Materials Science: Materials in Electronics*, **22**(7), 821-824 (2011).
10. Krishnamoorthy T., Thavasi V. and Ramakrishna, S. A first report on the fabrication of vertically aligned anatase TiO_2 nanowires by electrospinning: Preferred architecture for nanostructured solar cells. *Energy & Environmental Science*, **4**(8), 2807-2812 (2011).
11. Murari K., Kumar R., Kailasnath M., Radhakrishnan P. and Nampoori V. P. N., Optical characterization of ZnO nanoparticles and nanorods prepared by wet chemical technique at low temperature. *International Society for Optics and Photonics,* Vol. 7610, 761011(2010).
12. Vetrivel V., Rajendran K., and Kalaiselvi V., Synthesis and characterization of pure titanium dioxide nanoparticles by sol-gel method. *Int. J. ChemTech Res*, **7,** 1090-1097(2015).
13. Hedayati K., Fabrication and Optical Characterization of Zinc Oxide Nanoparticles Prepared via a Simple Sol-gel Method. *Journal of Nanostructures*, **5**(4), 395-401(2015).
14. Ristić M., Musić S., Ivanda M. and Popović S., Sol–gel synthesis and characterization of nanocrystalline ZnO powders. *Journal of Alloys and Compounds*, **397**(1-2), L1-L4(2005).
15. Mahmoud F. A., Shehata A. B., Mohamed H. and Magdy W., Organic-Inorganic Solar Cell Based on Sprayed MEH-PPV/ZnO Nanorods Layers. *Advanced Materials Research*, **896,** 489-492 (2014).
16. Ltaief A., Bouazizi A., Davenas J., Chaabane R. B. and Ouada, H. B., Electrical and optical properties of thin films based on MEH-PPV/ fullerene blends. *Synthetic Metals*, **147**(1-3), 261-266(2004).
17. Hasnidawani J. N., Azlina H. N., Norita H., Bonnia N. N., Ratim S. and Ali, E. S., Synthesis of ZnO nanostructures using sol-gel method. *Procedia Chemistry*, **19,** 211-216(2016).
18. Sharma A., Karn R. K. and Pandiyan S. K., Synthesis of TiO_2 nanoparticles by sol-gel method and their characterization. *J. Basic Appl. Eng. Res*, **1**(9), 1-5(2014).
19. Omer B. M., Optical properties of MEH-PPV and MEH-PPV/[6, 6]-Phenyl C61-butyric Acid 3-ethylthiophene ester thin films. *Journal of Nano-And Electronic Physics,* **4**(4), 04006(4pp)(2012).
20. Habelhames F., Wided Z., Lamiri L., Nessark B. and Derbal-Habak H., Morphology and photoelectrochemical characterization of MEH-PPV/PCBM composite film doped with TiO_2

nanoparticles. *Acta Metallurgica Sinica (English Letters)*, **26**(4), 373-377(2013).

21. Al-Algawi S. D., Rasheed R. T. and Rhoomi Z. R., Structural and Optical Properties of Annealed TiO_2 Powder Synthesized by Hydrothermal Method. *Iraqi Journal of Science*, **58**(3C), 1683-1693(2017).

22. Azar Sadollahkhani, Iraj Kazeminezhad, Jun Lu, Omer Nur, Lars Hultman and Magnus Willander, Synthesis, structural characterization and photocatalytic application of ZnO@ZnS coreshell nanoparticles, *RSC Adv.,* , **4,** 36940–36950 (2014).

23. Bi D., Wu F., Yue W., Qu Q., Cui Q., Qiu Z., Liu C., Shen W. and Wang M., Improved performance of MEH-PPV/ZnO solar cells by addition of lithium salt. *Solar Energy*, **85**(11), 2819-2825(2011).

24. Huang T., Jin B., Peng R. F., Chen C. D., Zheng R. Z., He Y. and Chu S. J., Synthesis and characterization of [60] fullerene-glycidyl azide polymer and its thermal decomposition. *Polymers*, **7**(5), 896-908(2015).

25. Grujić-Brojčin M., Šćepanović M. J., Dohčević-Mitrović Z. D., Hinić I., Matović B., Stanišić G. and Popović, Z. V., Infrared study of laser synthesized anatase TiO_2 nanopowders. *Journal of Physics D: Applied Physics*, **38**(9), 1415(2005).

26. Bomila R. and Srinivasan S., Synthesis and Characterization of ZnO Nanoparticles by Wet Chemical Method. *International Journal of Chem. Tech Research*, **7,** 3109-3114(2015).

27. Giri P. K., Bhattacharyya S., Singh D. K., Kesavamoorthy R., Panigrahi B. K. and Nair K. G. M., Correlation between microstructure and optical properties of ZnO nanoparticles synthesized by ball milling. *Journal of Applied Physics*, **102**(9), 093515(2007).

28. Gayathri S., Ghosh O. N., Sathishkumar S., Sudhakara S., Jayaramudu J., Ray S. S. and Viswanath A. K., Investigation of physicochemical properties of Ag doped ZnO nanoparticles prepared by chemical route. *Appl. Sci. Lett.,* **1**(1), 8-13(2015).

29. Zhang H., Zhou M., Fu Q., Lei B., Lin W., Guo H., Wu M. and Lei, Y., Observation of defect state in highly ordered titanium dioxide nanotube arrays. *Nanotechnology***, 25**(27), 275603(2014).

30. Kripal R., Gupta A. K., Srivastava R. K. and Mishra S. K., Photoconductivity and photoluminescence of ZnO nanoparticles synthesized via co-precipitation method. *Spectrochimica Acta Part A: Molecular and Biomolecular Spectroscopy*, **79**(5), 1605-1612(2011).

31. Yang S. H., Nguyen T. P. and Hsu C. S., Fabrication of MEH-PPV/SiO_2 and MEH-PPV/TiO_2 nanocomposites with enhanced luminescent stabilities. *Rev.Adv.Mater.Sci*. **15,** 144-149(2007).

32. Singh P., Kumar A., Kaushal A., Kaur D., Pandey A. and Goyal R. N., In situ high temperature XRD studies of ZnO nanopowder prepared via cost effective ultrasonic mist chemical vapour deposition. *Bulletin of Materials Science,* **31**(3), 573-577(2008).

33. Enesca A., Andronic L., Duta A. and Manolache, S., Optical properties and chemical stability of WO_3 and TiO_2 thin films photocatalysts. *Romanian Journal of Information Science and Technology,* **10**(3), 269-277(2007).

(*Received* 20/8/2018;
accepted 25/9/2018)

الخواص الضوئية لافلام البولي [-2ميثوكسي 5- (-2إيثيل هسيكلوكسي-ف- فينيل-فينيلن) مع ال C_{60}, مخلوط البولي [-2ميثوكسي 5- (-2إيثيل هسيكلوكسي-ف- فينيل-فينيلن) مع ال C_{60} و اكسيد التايتنيوم و مخلوط البولي [-2ميثوكسي 5- (-2إيثيل هسيكلوكسي-ف- فينيل-فينيلن) مع ال C_{60} و اكسيد الزنك

فوزي عبد الحميد محمود[١]، اسلام احمد محمد العزب[٢]، أسامة محمود ابو العنين[٣]، احمد عبد الفتاح[٢]، عادل أحمد محمد أحمد[٢]

[١]قسم فيزياء الجوامد - المركز القومي للبحوث - القاهرة - مصر.

[٢]قسم الكيمياء - كلية العلوم - جامعة حلوان - القاهرة - مصر.

[٣]قسم الاستخدامات البترولية - معهد بحوث البترول - القاهرة - مصر.

في هذا العمل، تم تحضير اكاسيد التيتانيوم و الزنك بطريقة السول جيل. وتم دراسة الخصائص الهيكلية والمورفولوجية والضوئية لكل منهما. من خلال استخدام تقنية حيود الأشعة السينية فقد تاكد تكون الشكل السداسي لاكسيد الزنك كما تكون طورين من اطوار اكسيد التايتنيوم وهما اناتيز بنسبة (85%) و روتيل بنسبة (15%). كما تكونت المواد في شكل كريستالات وهو ما تم تاكيدة من خلال تقنية حيود الأشعة السينية و الرامان الطيفي. و تم حساب احجام الجزيئات المكونة بالاعتماد علي معادلة شيرر ووجد انها متماشية مع النتائج التي تم الحصول عليها من خلال نتائج المجهر الالكتروني. تم حساب فرق الطاقة بين اخر مستوي مملوء بالالكترونات (HOMO) و اول مستوي فارغ من الالكترونات (LUMO) لكل من المواد عن طريق علاقة ال Kubelka-Munk باستخدام الانعكاسات المنتشرة في جميع الاتجاهات لكل مادة. و وجد ان الفرق بين هاذان المستويان بالنسبة لاكسيد الزنك و اكسيد التايتنيوم هو3.4 eV و 3.2 eV علي التوالي. تم اذابة البولي [2-ميثوكسي -5 (2-إيثيل هسيكلوكسي-ف- فينيل-فينيلن) الذي سمي بـ MEH-PPV مع C60 و تكوين فلم رقيق منه علي شرائح الزجاج. و تم دراسة الخصائص الهيكلية والمورفولوجية والضوئية لهذا الفيلم الرقيق. كما تم دراسة تاثير استخدام اكاسيد التايتنيوم و الزنك علي الخواص الفيزيائية لمخلوط البولي [2-ميثوكسي -5 (2-إيثيل هسيكلوكسي-ف- فينيل-فينيلن) MEH-PPV مع ال C60. و في النهاية تم تحليل جميع النتائج للتحقق من إمكانية استخدام هذه الطبقات كطبقة امتصاص لتطبيقات الطاقة الشمسية.